# REPORT DOCUMENTATION PAGE

| 1. REPORT DATE *(DD-MM-YYYY)* | 2. REPORT TYPE | 3. DATES COVERED *(From - To)* |
|---|---|---|
| 04 January 2016 | Conference Paper | 12 November 2015 – 04 January 2016 |

| 4. TITLE AND SUBTITLE | | 5a. CONTRACT NUMBER |
|---|---|---|
| Application of Detailed Chemical Kinetics to Combustion Instability Modeling | | |
| | | 5b. GRANT NUMBER |
| | | 5c. PROGRAM ELEMENT NUMBER |
| 6. AUTHOR(S) | | 5d. PROJECT NUMBER |
| Harvazinski, M., Talley, D., Sankaran, V. | | |
| | | 5e. TASK NUMBER |
| | | 5f. WORK UNIT NUMBER |
| | | Q0A1 |

| 7. PERFORMING ORGANIZATION NAME(S) AND ADDRESS(ES) AND ADDRESS(ES) | 8. PERFORMING ORGANIZATION REPORT NO. |
|---|---|
| Air Force Research Laboratory (AFMC) AFRL/RQRC 10 E. Saturn Blvd. Edwards AFB, CA 93524-7680 | |

| 9. SPONSORING / MONITORING AGENCY NAME(S) AND ADDRESS(ES) | 10. SPONSOR/MONITOR'S ACRONYM(S) |
|---|---|
| Air Force Research Laboratory (AFMC) AFRL/RQR 5 Pollux Drive Edwards AFB, CA 93524-7048 | |
| | 11. SPONSOR/MONITOR'S REPORT NUMBER(S) |
| | **AFRL-RQ-ED-TP-2015-418** |

**12. DISTRIBUTION / AVAILABILITY STATEMENT**

Approved for public Release; distribution unlimited

**13. SUPPLEMENTARY NOTES**

For presentation at AIAA SciTech 2016; San Diego, CA (04 January 2016)
PA Clearance Number 15692 Clearance Date 12/3/2015

**14. ABSTRACT**

A comparison of a single step global reaction and the detailed GRI-Mech 1.2 for combustion instability modeling in a methane-fueled longitudinal-mode rocket combustor was performed. A single element shear-coaxial injector was operated under two different conditions corresponding to marginally stable and unstable operation in order to evaluate the performance of the chemical kinetics mechanisms on combustion stability. Results show improved prediction in the frequencies and amplitudes with the detailed kinetics but the underlying source of the instability phenomena remains the same. In contrast to previous two-dimensional results, these three-dimensional results demonstrate that the present non-premixed injector configuration is primarily mixing-controlled and that the global chemical kinetics are sufficient to capture the stability characteristics.

**15. SUBJECT TERMS**

N/A

| 16. SECURITY CLASSIFICATION OF: | | | 17. LIMITATION OF ABSTRACT | 18. NUMBER OF PAGES | 19a. NAME OF RESPONSIBLE PERSON D. Talley |
|---|---|---|---|---|---|
| a. REPORT Unclassified | b. ABSTRACT Unclassified | c. THIS PAGE Unclassified | SAR | 17 | 19b. TELEPHONE NO *(include area code)* N/A |

# Application of Detailed Chemical Kinetics to Combustion Instability Modeling

Matthew E. Harvazinski,* Douglas G. Talley,† and Venkateswaran Sankaran‡

*Air Force Research Laboratory, Edwards AFB, CA, 93524*

**A comparison of a single step global reaction and the detailed GRI-Mech 1.2 for combustion instability modeling in a methane-fueled longitudinal-mode rocket combustor was performed. A single element shear-coaxial injector was operated under two different conditions corresponding to marginally stable and unstable operation in order to evaluate the performance of the chemical kinetics mechanisms on combustion stability. Results show improved prediction in the frequencies and amplitudes with the detailed kinetics but the underlying source of the instability phenomena remains the same. In contrast to previous two-dimensional results, these three-dimensional results demonstrate that the present non-premixed injector configuration is primarily mixing-controlled and that the global chemical kinetics are sufficient to capture the stability characteristics.**

## I.   Introduction

COMBUSTION instability is a complex interaction between acoustics and the heat release due to combustion. In rocket engines, which are acoustically compact, there is significant potential for instabilities to arise. Instabilities can lead to performance issues or result in catastrophic failure and have plagued rocket engine design leading back to the development of the F-1 engine in the 1960s.[1] Recent work using large eddy simulations (LES) or detached eddy simulations (DES) have shown the ability to capture combustion instability with computational fluid dynamics (CFD) simulations of reacting flow in single-element (longitudinal-mode) and multi-element (transverse-mode) laboratory scale rocket combustors.[2–5] The majority of these simulations have used simplified chemical kinetics, typically single step or two-step mechanisms, to model the methane combustion.[6,7] These studies have been instrumental in describing the qualitative physical phenomena underlying the occurrence of combustion instabilities in these rocket combustors and have been able to correctly predict both stable and unstable behavior as a function of injector design. However, precise quantitative prediction of the modal frequencies and amplitudes remains a challenge. The present article is an attempt towards addressing such discrepancies by enhancing the chemical kinetics model used in the calculations.

It is well known that these approximate global mechanisms are incapable of predicting ignition delay times and the correct heat release rate over a wide range of equivalence ratios and operating conditions. The reacting flowfield in the vicinity of an injector contains large variations in the mixedness of the oxidizer, fuel, and products, which suggest that the global mechanisms may be insufficient to accurately capture the combustion in this region. Previous studies have shown that a determining factor in the stability behavior of the injector is the timing between injector/chamber acoustics and the mixing/combustion processes, which means that the ignition delay can have a significant effect. Moreover, two-dimensional studies using detailed chemical kinetics in a longitudinal-mode chamber have shown that the kinetics can strongly impact the nature of the stability predictions.[8] The present study is motivated by the desire to extend these detailed kinetics studies to three-dimensional simulations which are necessary to correctly capture the time-scale balance between fuel-oxidizer mixing, combustion and acoustics.

The reliance on simplified mechanisms in combustion stability calculations is mainly due to computational cost, especially in an LES or DES context, which can involve long-time integrations. Even a compact detailed

---

*Research Aerospace Engineer, AIAA Member.
†Principal Research Physical Scientist, AIAA Associate Fellow.
‡Senior Scientist, AIAA Senior Member.

American Institute of Aeronautics and Astronautics

kinetics mechanism contains upwards of 30 chemical species and hundreds of reactions. In a detailed non-equilibrium simulation, individual conservation equations must be solved for each species. Thus, as the number of species increases so does the size of the system. The resulting matrix and vector operations become costly; comparing a global mechanism with 5 species and a detailed mechanism with 31 species, the respective system sizes are 12 and 38 equations. Operations like matrix multiplication scale with $N^3$, resulting in a 32 times increase in computational cost (although modern cache sizes help reduce this effect somewhat). Increased loop size in the computation of thermodynamic and transport properties can also have a substantial impact on the computational cost. Moreover, large numbers of reactions increase the cost by directly impacting the number of operations that must be performed at each cell and each time step in order to compute the species production term. Therefore, chemical mechanisms that are originally designed for zero- or one-dimensional simulations can become intractable for multi-dimensional unsteady CFD simulations with millions of cells.

Many combustion calculations adopt compact chemistry representations such as flamelets, wherein the individual species compositions are tabulated in terms of a mixture fraction and (usually) a reaction progress variable obtained from a generic flame configuration such as a counter-flow diffusion flame. In this manner, large chemical kinetics systems can be pre-solved and stored in tabular form. The approach, however, has some difficulties. For instance, the flamelet equations neglect compressibility effects and represent the solution in terms of a few parameters corresponding to the injection conditions of the fuel and oxidizer.[9] As a consequence, acoustic coupling effects and local interactions that arise due to heat transfer, turbulence, flow recirculation and so on are not properly accounted for. Moreover, to represent the correct speed of sound in the combustor, it is necessary to solve the full form of the energy equation in the resolved LES scale in addition to the more approximate energy equation solution that is tabulated. The solutions obtained from these two forms of the energy equation are often inconsistent and the difference in the two solutions is an indicator of the error in the tabulated species results. Another limitation is that capturing the instability of the flame anchoring point and the dynamics of lifted flames require a degree of calibration that challenges the application of these methods for combustion instability predictions. In fact, the authors are not aware of successful attempts of predicting combustion instability phenomena in rocket combustors using flamelet-based combustion models. For these reasons, we do not invoke the flamelet assumption in this study and, instead, adopt individual transport equations to represent the chemical species present.

Turbulent combustion closure is another aspect of reacting-LES or DES flame calculations. Our previous studies have included both a simple laminar combustion model (LCM) as well as turbulent combustion closure using the linear eddy model (LEM).[10] The results indicate that for the non-premixed diffusion flames that characterize these rocket combustors, the inclusion of the turbulent combustion model has little impact on the combustion instability predictions. Moreover, the use of the LEM even with global chemical kinetics is several times more computationally expensive than the corresponding LCM calculation and would be prohibitive when used with detailed chemical kinetics. Here, we therefore retain the use of LCM, which, in our view, will not materially affect the predictive results.

The present work studies the single-element gas-gas injector operating in a longitudinal-mode rocket combustor with methane as the fuel. We use the GRI-Mech 1.2 kinetics mechanism for methane oxidation.[11] The GRI-Mech 1.2 was chosen over 2.11 because the only change between 1.2 and 2.11 is the addition of nitrogen chemistry and the present simulations do not contain nitrogen.[12] While version 3.0 should produce improved results over 1.2, it is nearly twice the size of 1.2 and was therefore deemed unaffordable.[13] For this study, two operating conditions are chosen which have shown discriminating stability behavior both experimentally and in prior computational work utilizing global chemistry.[6] Before presenting the prediction results, we provide some additional experimental and computational background in the next section.

## II.   Background

A large body number of simulations of the continuously variable resonance chamber (CVRC) experiment[14] has already been completed and is therefore selected for the present investigation. The experimental apparatus is shown in Figure 1. The setup is a single element shear coaxial injector, the fuel is gaseous methane and decomposed hydrogen peroxide is used for the oxidizer. The combustor is a fixed length of 38.1 cm with a choked converging-diverging nozzle affixed to the downstream end. The oxidizer post length is varied using a linear actuator. At short injector post-lengths, the behavior is characterized as marginally stable with peak-to-peak pressure fluctuations on the order of 160 kPa (12% $p_c$). At intermediate post-lengths,

the most unstable is observed with peak-to-peak pressure fluctuations on the order of $400\,\mathrm{kPa}$ ($30\%$ $p_c$). As the post-length is further increased, the combustion becomes stable but the actual length, that this occurs at, has shown variability in the experiments. For this study the marginally stable short length, $8.89\,\mathrm{cm}$, and the intermediate unstable length, $13.97\,\mathrm{cm}$, are selected for investigation. Both of these lengths have been simulated in the past by several researchers.[2, 4, 9]
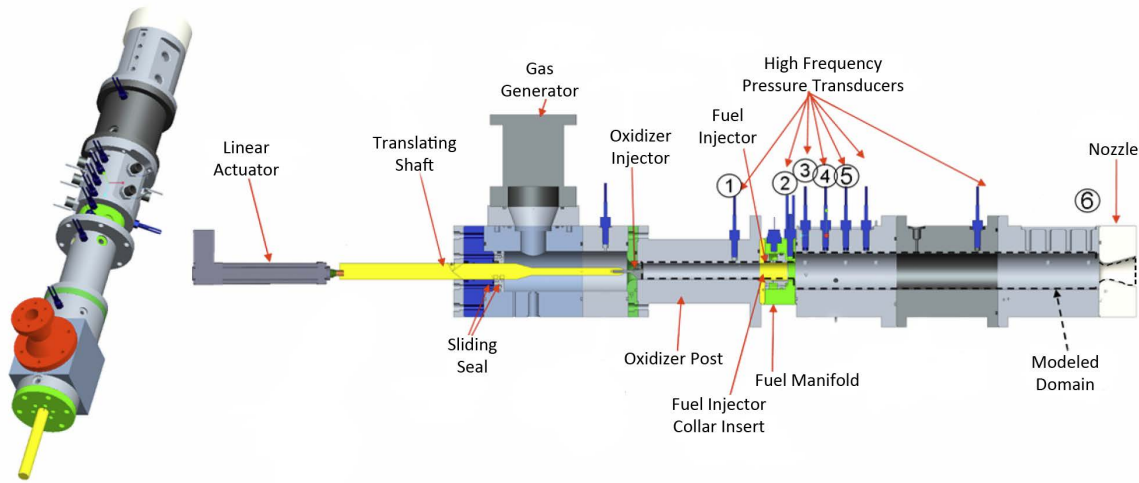


Figure 1: Experimental configuration of the CVRC experiment.

A series of three-dimensional simulations using a single step global mechanism produced results that agree well with the experimental results, especially for the marginally stable case.[2] These results have been useful in predicting the underlying physics that lead to stable and unstable operation of this combustion. However, some significant discrepancies remain with the computational results for the unstable case with the frequencies being over-predicted by about 10-15% and the amplitudes under-predicted by 30-50% (depending on the mode). It is of interest to see if these discrepancies may be influenced by the chemical kinetics of the methane oxidation.

Two-dimensional results with global chemistry have shown significantly lower amplitudes than the experiments and the three-dimensional computations.[15] More recently, two-dimensional results using the GRI-Mech 1.2 mechanisms have shown much better agreement with the experimental results. Amplitudes increased to levels comparable to the three-dimensional global results for the unstable length. It was postulated that the timing of the combustion was off in the two-dimensional global kinetics simulations. By using detailed kinetics, the combustion occurred in sync with the chamber acoustics resulting in a stronger coupling and larger amplitudes.[8] However, we note that the three-dimensional results with global kinetics are able to achieve good agreement and, therefore, this explanation may be simplistic. In fact, the limitations of two-dimensional mixing may be leading to a more important role for the chemical kinetics. The present studies with three-dimensional detailed kinetics are expected to provide a more physically accurate picture of the relative roles of mixing and combustion and their interactions with the chamber acoustics.

It is instructive to review the current state-of-the-understanding of the instability mechanisms in this longitudinal chamber experiment and to compare these physics to the corresponding simulations with detailed chemical kinetics. Specifically, the stability characteristics are governed by the timings of the pressure waves in the oxidizer post and the combustor. In the unstable case, the lengths are such that the reflected pressure wave in the oxidizer post arrives in the combustor just before the reflected wave in the combustor. These events lead to a synchronization of the time of maximum combustion with the acoustic wave period in the chamber, thereby amplifying the modes. Alternately, in the case of the stable combustion, the timing of these waves are out of sync and the reflected wave in the post returns to the combustor head-end well in advance of the wave in the combustor itself. This results in a more continuous heat release throughout the acoustic cycle and less opportunity for coupling with the chamber acoustics, leading in turn to more stable operation. A complete description of the behavior is available in Ref. 2.

Like the previous three-dimensional global kinetics studies and the recent two-dimensional chemical kinetics studies, the simulations are carried out with the GEMS code. It is an unstructured Navier-Stokes code

American Institute of Aeronautics and Astronautics

that uses the $k$-$\omega$ DES model for turbulence.[16–20] The present computations use the GRI-Mech 1.2 kinetics set. As mentioned previously, transport equations are solved for all chemical species and the combustion source term is closed with a laminar closure model (LCM). The code uses a dual-time formulation to ensure temporal accuracy and utilizes an implicit solver in the pseudo-time iterations.

# III. Results

Two operating conditions were modeled, a marginally stable and an unstable. Prior three-dimensional results showed excellent agreement using global kinetics for the marginally stable condition. The simulation for the unstable case predicted slightly lower amplitudes than were observed experimentally. A time step size of $0.1\,\mu$s was used and the mesh size was approximately 4 million cells. To reduce the mesh size, the complex oxidizer slots were approximated by a constant mass flow inlet. This was previously shown to have small effect on the primary instability mode and reduced the size of the mesh by approximately 20 percent.[21]

## A. Computational Costs

The detailed mechanism is significantly more expensive. The costs are summarized in Table 1. Global simulations were run with 960 cores for a total time of 40 ms, simulations with the detailed kinetics were run with 21,600 cores for a total time of 20 ms. For a 20 ms simulation 5.18 million hours were required when using the detailed kinetics compared to 0.23 million hours for the global mechanism. The detailed chemistry cases therefore required 22.5 times the CPU hours of the corresponding global cases.

Table 1: Computational costs

|  | Global | Detailed GRI-1.2 |
| --- | --- | --- |
| Number of reactions | 1 | 177 |
| Number of species | 4 | 31 |
| Number of cores | 960 | 21,600 |
| Core hours per ms | 11,520 | 259,200 |

## B. Pressure Time History

The initial transient for the simulations is different. Figure 2 shows the first 14 ms for the two simulations of the unstable operating condition. Similar trends are observed in the marginally stable operating point. The first noticeable difference is the immediate rise in the chamber pressure at the start of the simulation for the detailed case. This is because the chamber is initially filled with warm combustion products at 1500 K. The detailed kinetics set contains additional reactions that are active under these conditions, which results in a uniform rise in the pressure, temperature and a change in the combustion products as solution reaches a new equilibrium condition. Aside from this offset in the mean pressure, the initial transient is similar through the first 2.2 ms. After that the global simulation experiences a rapid rise in the pressure as sufficient methane has accumulated in the combustor to ignite. This rapid rise in pressure occurs later for the detailed kinetics—closer to 4 ms from the start of the simulation. The behavior after ignition is also different for the two cases, with the global case showing a rapid drop in amplitude followed by a ramp-up before reaching the limit cycle. The detailed chemistry exhibits a smooth decay in amplitude from the ignition spike to the final limit cycle amplitude. However, we note that the limit cycle amplitudes are remarkably similar for the two mechanisms.

The fluctuating pressure for all four simulations is shown in Figure 3. For both operating conditions the amplitudes of the peak-to-peak pressure are higher when using the detailed chemistry. The difference is more pronounced for the unstable operating point where the cycle-to-cycle amplitude shows less cycle to cycle variability. The mean pressure (averaged from 5 ms to 20 ms) increases slightly with the detailed chemistry. For the marginally stable case the mean pressure increases to 155.4 kPa from 154.6 kPa, while for the unstable case, the mean pressure increases to 156.8 kPa from 153.1 kPa. The overall behavior is similar for both mechanisms. Consistent with the experimental results the marginally stable operating point shows

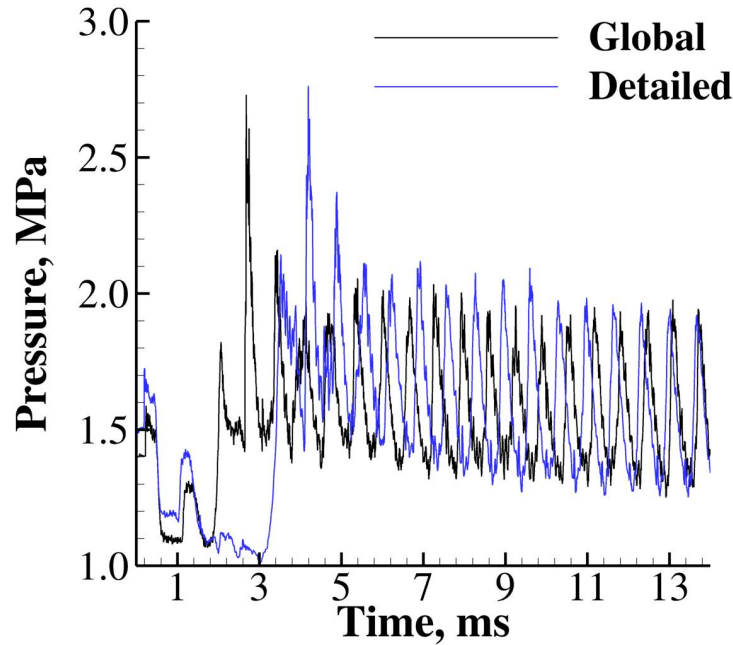American Institute of Aeronautics and Astronautics

Figure 2: Initial pressure time history for the unstable operating point. The first 15 ms of data are shown.

more cycle-to-cycle variability. While the unstable operating condition locks onto the limit cycle amplitude quickly and shows steep fronted waves in both cases. The spike, located at the trough of the cycle and associated with reignition of the unburned methane in the combustor, is larger for the detailed mechanism and is examined further in the cycle analysis section.

## C.    Power Spectral Density Analysis

The raw and fluctuating pressure data shows that larger amplitudes are present with the detailed kinetics. More detailed information can be obtained using a power spectral density (PSD) analysis of the pressure. The PSD plots are shown in Figure 4. This analysis is performed on the unsteady pressure signal for all four simulations and the corresponding experimental results. The simulation runtime using the detailed chemistry was half that of the global mechanism because of the excessive computational cost. This affects the frequency resolution and sharpness of the peaks. For the global mechanism 35 ms of data were used resulting in a frequency resolution ±28.57 Hz. For the detailed mechanism only 15 ms of data were used resulting in a frequency resolution of ±66.67 Hz. It is expected with additional run time the PSD peaks would become sharper slightly altering the identified frequencies and corresponding amplitudes.

Quantitative data for the PSDs are shown in Table 2 for the marginally stable operating condition and Table 3 for the unstable operating condition. The PSD data is interrogated using a full-width half-max integration to extract the power associated with the peaks in the plot.[22]    Again, because of the shorter run time for the detailed chemistry the frequencies and resulting amplitudes may change slightly if the analysis repeated with additional data but the general trends are expected to remain the same. In both cases the frequency of first mode with the detailed kinetics simulations is lower compared to the frequency predicted by the simulations based on the global mechanism. However, the frequencies remain higher than the experimental results. It is believed that the remaining discrepancy between the simulation and experimental frequencies is due to the treatment of the thermal wall boundary condition. In the experiments the thermal mass associated with the wall will act as a heat sink removing energy from the combustor. Simulations treat the wall boundary as an adiabatic wall due to a lack of heat flux data from the experiment. Amplitudes are consistently higher for the detailed chemistry simulations. There is however less of a difference in the amplitudes between the two mechanisms than was previously reported for the two-dimensional study.[8]

American Institute of Aeronautics and Astronautics
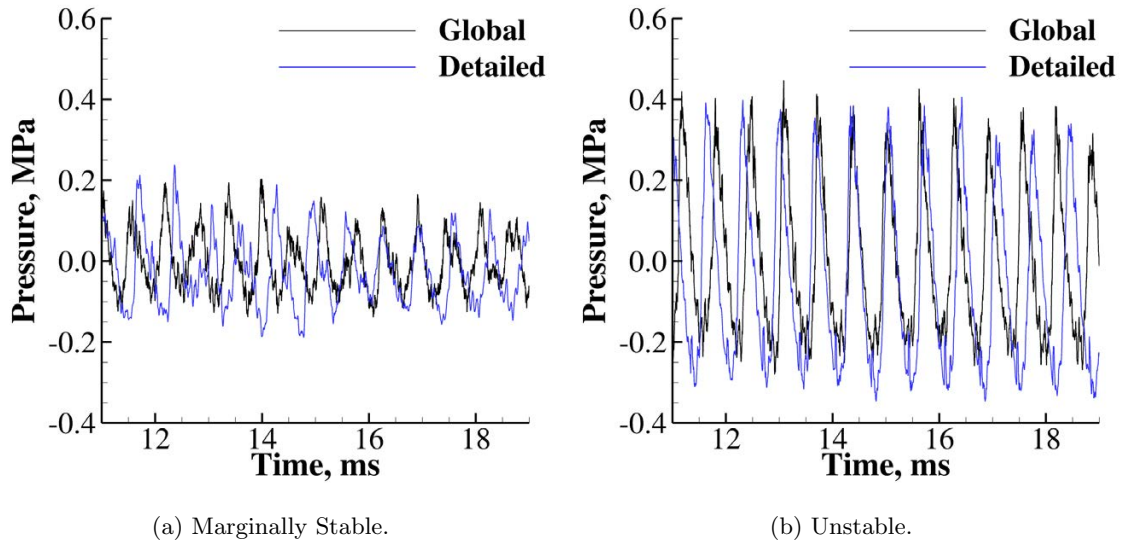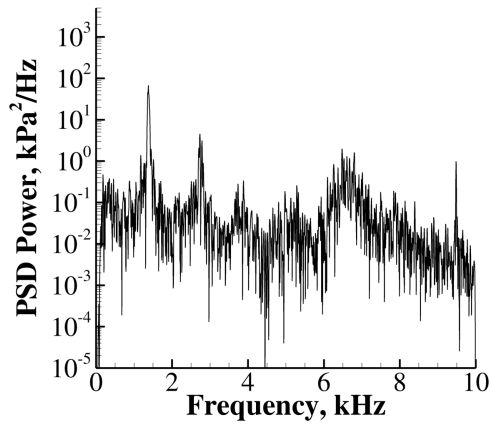
(a) Marginally Stable.

(b) Unstable.

Figure 3: Fluctuating pressure comparison for both operating conditions.

Table 2: Marginally stable PSD results showing the amplitude and frequency for the experiment and the two simulations.
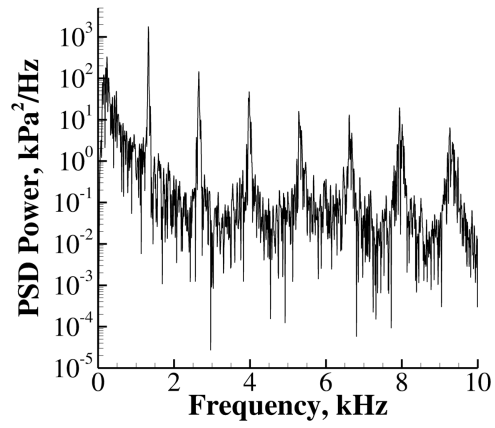
| Mode | Experiment | | | Global | | | Detailed | | |
|---|---|---|---|---|---|---|---|---|---|
| | $f$, Hz | $p'_{ptp}$, kPa | $f_i/f_1$ | $f$, Hz | $p'_{ptp}$, kPa | $f_i/f_1$ | $f$, Hz | $p'_{ptp}$, kPa | $f_i/f_1$ |
| 1 | 1379 | 121.70 | 1.00 | 1714 | 129.54 | 1.00 | 1533 | 146.65 | 1.00 |
| 2 | 2734 | 5.86 | 1.98 | 3428 | 20.57 | 1.98 | 2733 | 73.12 | 1.78 |
| 3 | 3882 | 16.03 | 2.82 | 4429 | 27.57 | 2.58 | 4200 | 36.37 | 2.74 |

Table 3: Unstable PSD results showing the amplitude and frequency for the experiment and the two simulations.

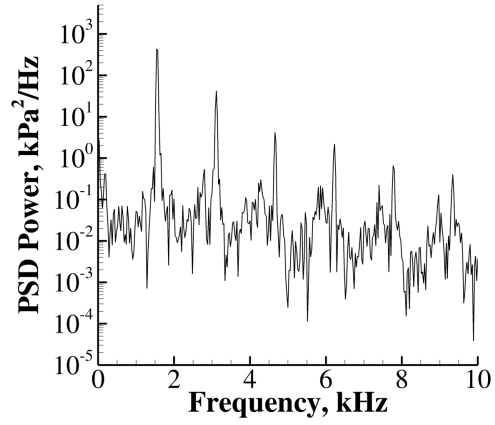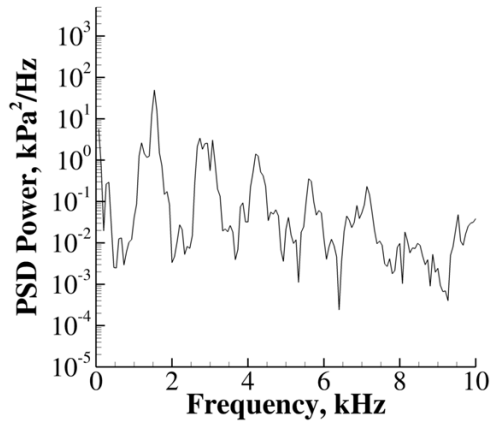| Mode | Experiment | | | Global | | | Detailed | | |
|---|---|---|---|---|---|---|---|---|---|
| | $f$, Hz | $p'_{ptp}$, kPa | $f_i/f_1$ | $f$, Hz | $p'_{ptp}$, kPa | $f_i/f_1$ | $f$, Hz | $p'_{ptp}$, kPa | $f_i/f_1$ |
| 1 | 1324 | 387.15 | 1.00 | 1543 | 349.10 | 1.00 | 1467 | 416.79 | 1.00 |
| 2 | 2655 | 89.29 | 2.01 | 3114 | 87.55 | 2.01 | 2933 | 130.41 | 2.00 |
| 3 | 3979 | 46.37 | 3.01 | 4629 | 36.25 | 3.00 | 4400 | 64.88 | 3.00 |

(a) Marginally Stable, Experiment
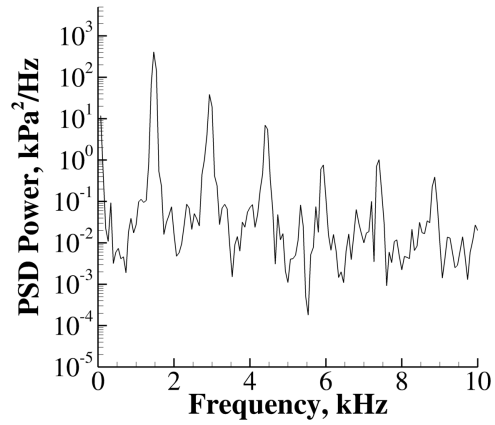
(b) Unstable, Experiment.
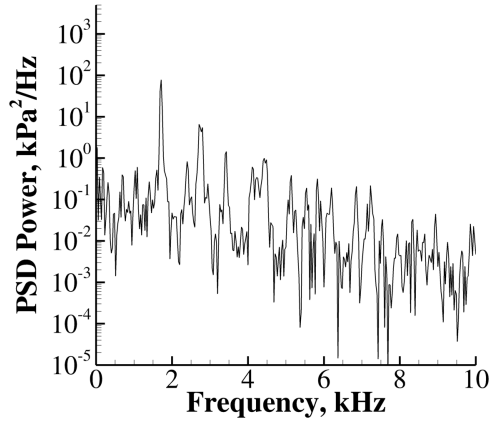
(c) Marginally Stable, Global

(d) Unstable, Global.

(e) Marginally Stable, Detailed

(f) Unstable, Detailed.

Figure 4: PSD plots for the experimental and computational results.

## D. Average Results

Table 4 shows the time averaged combustion products and temperature at the downstream location for the unstable case. The detailed chemistry has slightly more fuel left and about 1% more $O_2$ remaining. The concentrations of $H_2O$ and $CO_2$ are both lower for the detailed chemistry. The detailed mechanism also as a large number of species present with trace concentrations ($< 1 \times 10^{-5}$), the only two species not included in the global mechanism that are present with any significant value is OH and CO, both with mass fractions less than 1% each. The largest difference is in the temperature field which is 168 K lower for the detailed mechanisms. The differences in the species mass fraction and the temperature result in a sound speed that is 30 m/s lower. This is the source of the lower frequencies obtained in the PSD analysis. Similar differences in the mean quantities are observed at the marginally stable operating point.

Table 4: Downstream time-averaged combustor conditions. Mass fractions may not sum to unity because of rounding.

| Parameter | Global | Detailed |
|---|---|---|
| $CH_4$ | 0.00002 | 0.00003 |
| $O_2$ | 0.07239 | 0.08575 |
| $H_2O$ | 0.70679 | 0.69472 |
| $CO_2$ | 0.22063 | 0.20321 |
| OH | — | 0.00908 |
| CO | — | 0.00580 |
| Trace Species | — | $< 1 \times 10^{-5}$ |
| Temperature | 2495. K | 2327. K |
| Sound Speed | 1066.7 m/s | 1037.2 m/s |

## E. Cycle Analysis: Unstable Case

Representative cycles for each simulation have been selected for detailed analysis. The cycle of interest along with the identification of six examination points is shown in Figure 5 for the unstable operating point. The cycle start time is indicated by the dashed vertical line and corresponds to the instance when the head end is experiencing a pressure maximum. The cycle progress through the trough of the cycle and ends when the combustor head end pressure is again at a maximum (also indicated by a dashed vertical line). The total time for a single cycle is about 0.67 ms.

Six time instances of interest are indicated on each of the cycle plots, these were selected to occur with the same approximate spacing for each simulation and describe the flowfield at key times. Two sets of data will be shown for each point. The heat release contour is shown along with two isolines, the black isoline is the stoichiometric mixture fraction. The green line is an isotherm at 2000 K and demarcates the burnt and unburnt gases. The second series of images shows the fuel mass fraction contour along with colored isobar lines to identify the pressure.

The cycle analysis is split by mechanism so that it is easier to compare the contours for each a single simulation side by side. Figure 6 shows the detailed mechanism results and the global mechanism results are presented in Figure 7. For the first time instance, the pressure contour shows the pressure wave in the oxidizer post moving upstream away from the combustor. The global simulation shows significantly more accumulated fuel in the combustor while the detailed simulation has a trail of methane leading from the injection point, and some lingering methane away from the dump plane. No methane is present in corner where the dump plane and combustor wall meet. The heat release is qualitatively similar in both cases with a large amount of heat release taking place however the distribution is different. With detailed kinetics there is increased heat release taking place in the recirculation region near the wall downstream from the dump plane. There is also less heat intense heat release just downstream of the dump plane with the detailed mechanism, the most intense heat release is taking place further downstream. With the global kinetics the most intense heat release occurs just downstream of the dump plane suggesting that the global mechanism is operating similar to a "mixed is burned" scenario. Both simulations show some combustion in the cup

American Institute of Aeronautics and Astronautics
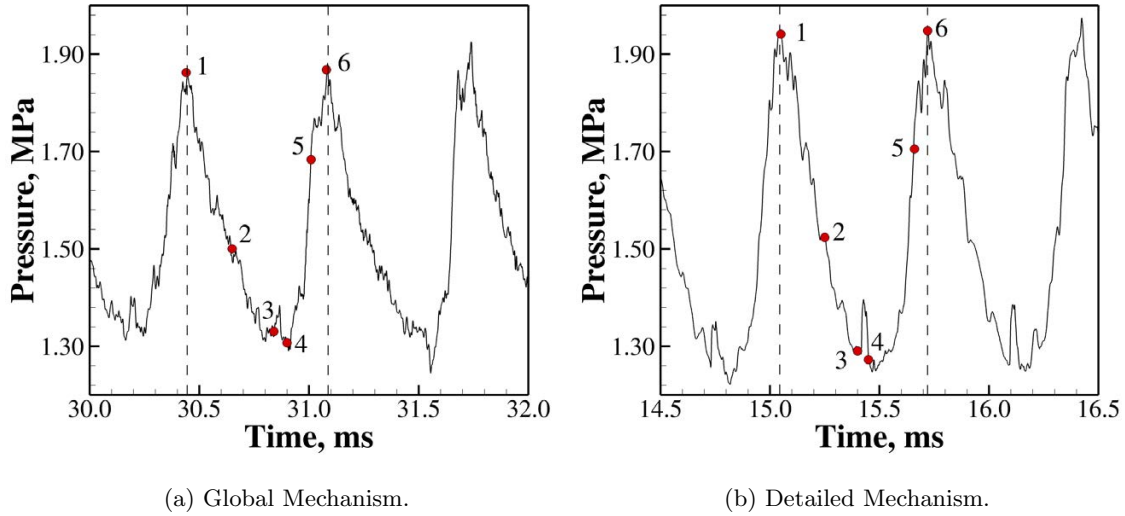
(a) Global Mechanism.  (b) Detailed Mechanism.

Figure 5: Cycle analysis points for the unstable configuration. The start and end times of the cycle are indicated by the dashed vertical lines. The red numbered points indicated the times of the detailed analysis.

region near the wall, but the fuel is largely absent from the near wall region, which is especially evident in the detailed simulation where fuel has been actually been pushed upstream of the injection plane by the high pressure wave in the oxidizer post.

At the second point in the cycle the pressure at the head end of the combustor has begun to rapidly decrease as is evident in the contour plot. There is also a significant amount of fuel accumulating in the shear layer region downstream of the dump plane. Comparing this region of fuel with the heat release map, we can see that very little of it is burning. Again, there is more methane present in the outer periphery of the combustor in the global simulation. The third point in the cycle is at the pressure minimum and occurs just before the oxidizer post wave has returned to the combustor. The returning pressure wave is visible in both cases and is about to enter the combustor. Notice that at this point the heat release is also at a minimum, there is very little heat release taking place. The large amount of methane that has accumulated shows that very little combustion is taking place.

The spike that is visible in the tough of the pressure trace in Figure 5 is the result of the pressure wave returning into the combustor. The pressure rise is larger for the detailed mechanism. The pressure contours show the wave expanding around the dump plane. In doing so, the wave pushes the accumulated fuel into the warm recirculating gases. In the case of the global mechanisms the reignition takes place in the vicinity of the dump plane shortly after it mixes with the warm recirculating gases. This does not appear to be the case for the detailed mechanism. Instead combustion takes place slightly later in the cycle, which may be responsible for the larger spike since more fuel has accumulated before the reignition event. Also, in the detailed case, we observe that the fuel is more concentrated, being restricted to the shear layer and not evident in the recirculation region.

Moving from time 4 to time 5, there is a rapid rise in the pressure. This is due to a combination of the returning acoustic wave in the combustor and the combustion taking place at the head end. The large amount of previously unburnt fuel at the head end is now rapidly burning as it mixes with the warm recirculating gases. The flowfields of both simulations show large regions of heat release primarily along the shear layer. With detailed chemistry there is more heat release in the recirculation region between the shear layer and combustor wall. Time six returns to the maximum pressure at the combustor head end. Here, we observe evidence of burning in the cup region and the ensuing disruption of the incoming fuel. The high-pressure in the combustor sends an acoustic wave into the oxidizer post, which in turn pushes the burning flow into the cup region and consumes a portion of the unburnt methane near the wall. The remaining fuel is displaced from the injection plane and pushed to the center of towards the center line. This fuel disruption is more severe in the case of the detailed chemistry.

Overall, the behavior of the detailed and global kinetics is very similar. Both show the fuel disruption

American Institute of Aeronautics and Astronautics

**(a) Time 1.** **(b) Time 1.**

**(c) Time 2.** **(d) Time 2.**

**(e) Time 3.** **(f) Time 3.**

**(g) Time 4.** **(h) Time 4.**

**(i) Time 5.** **(j) Time 5.**
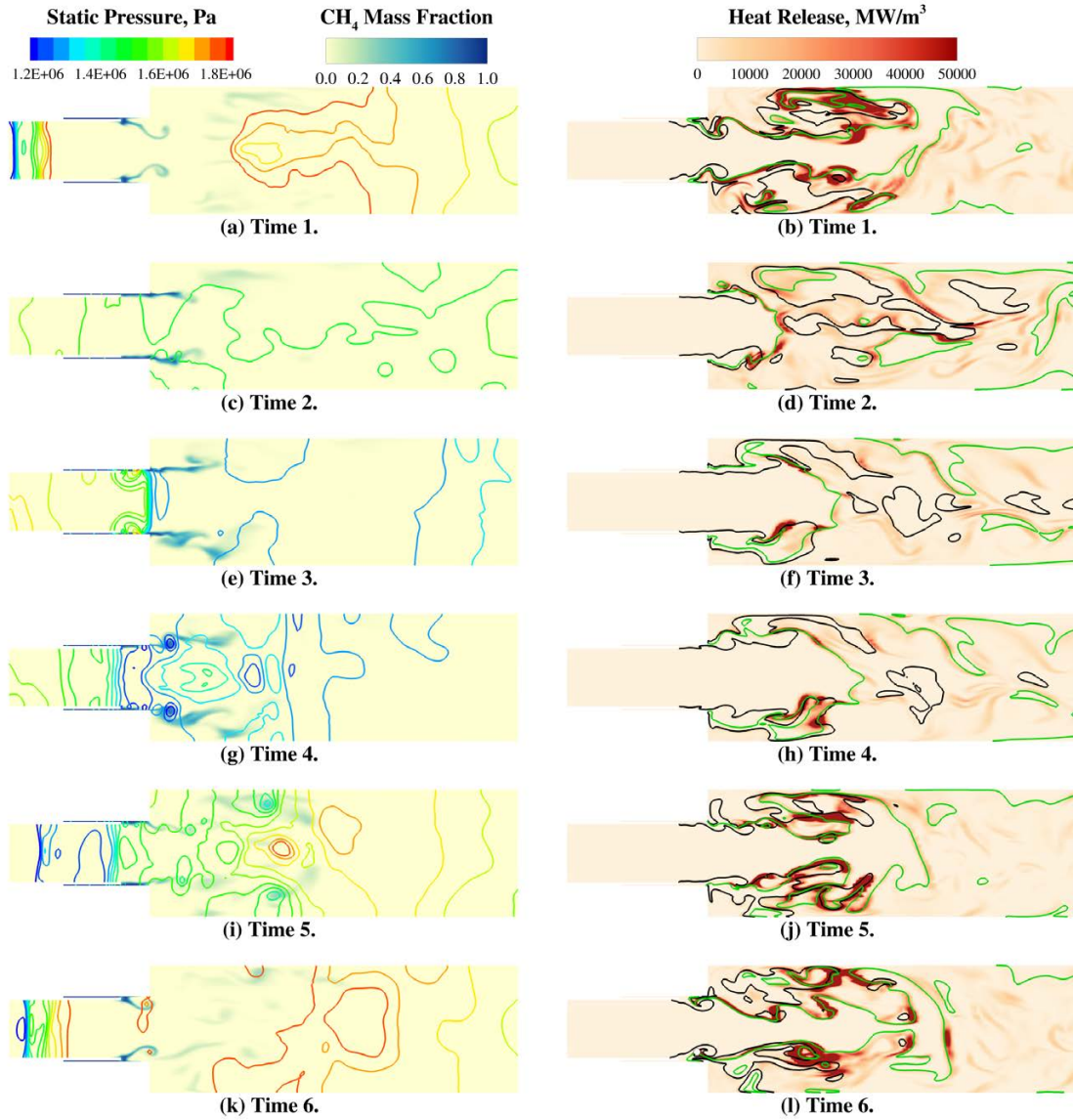
**(k) Time 6.** **(l) Time 6.**

Figure 6: Detailed cycle analysis for the detailed chemistry for the unstable operating point. Images on the left show the fuel mass fraction contour, the lines represent pressure isobars. The images on the right show the heat release contour. The green line is a 2000 K isotherm and the black line is the stoichiometric mixture fraction.
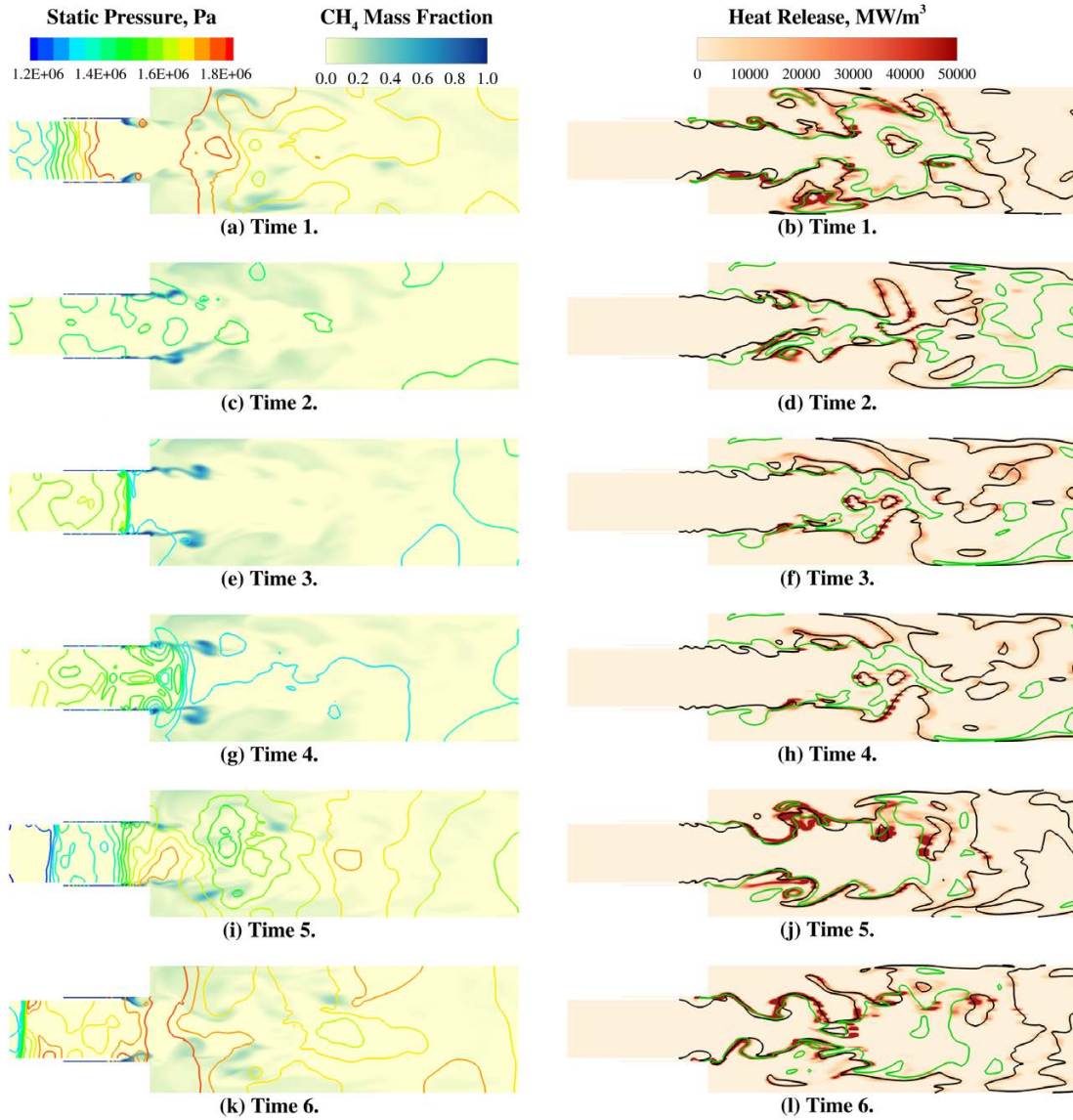
Figure 7: Detailed cycle analysis for the global chemistry for the unstable operating point. Images on the left show the fuel mass fraction contour, the lines represent pressure isobars. The images on the right show the heat release contour. The green line is a 2000 K isotherm and the black line is the stoichiometric mixture fraction.

and subsequent reignition in the second half of the cycle. The point of reignition is different; in the global case, it occurs close to the dump plane when the returning oxidizer pressure wave pushes the accumulated fuel into the warm recirculating gases. For the detailed mechanism, reignition occurs slightly later after mixing with the recirculating gases further downstream. Through the cycle the location of the heat release is different. The global mechanism shows heat release primarily along the shear layer, while the detailed mechanism shows significantly more heat release occurring in the recirculation region. There is also more lingering unburnt methane in the region near the wall for the global chemistry because of the difference in the heat release locations.

## F.   Cycle Analysis: Marginally Stable Case

Representative cycles for each simulation have been selected for detailed analysis. The cycle of interest along with the six examination points are shown in Figure 8. Plots identical to those shown for the unstable case are shown in Figure 9 and Figure 10 for the detailed and global kinetics respectively. Before considering the cycle analysis, it is interesting to note that the zoomed- in pressure trace shows significantly less noise for the detailed mechanism. This was reported previously for both the unstable and marginally stable case in the two-dimensional study.[8] This will be evident in the pressure plots, where this is more organization in the pressure waves with the detailed kinetics compared to the global kinetics in the oxidizer post.



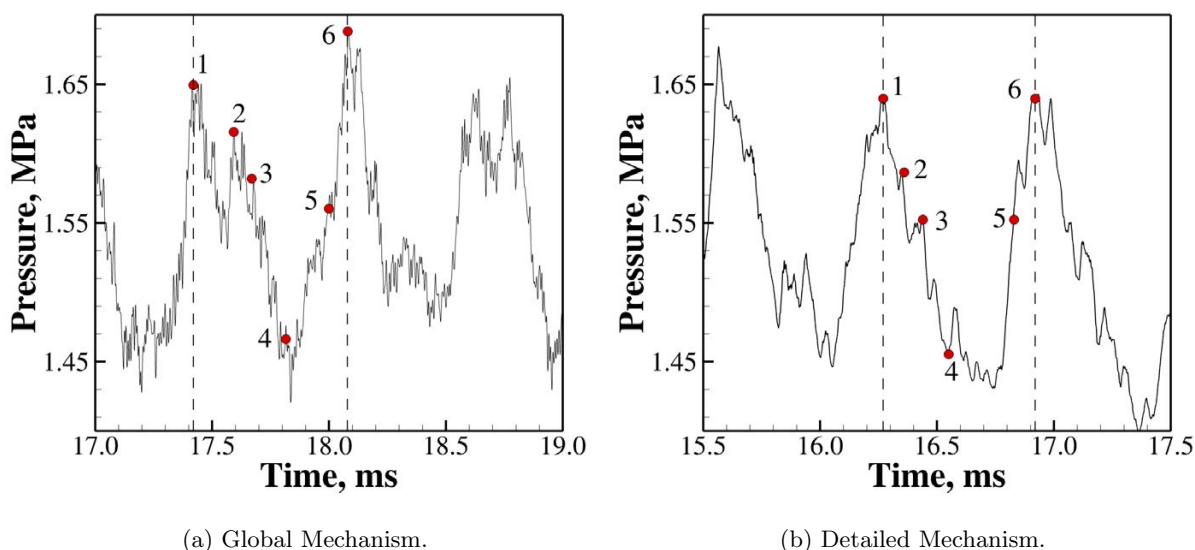(a) Global Mechanism.                                    (b) Detailed Mechanism.

Figure 8: Cycle analysis points for the unstable configuration. The start and end times of the cycle are indicated by the dashed vertical lines. The red numbered points indicated the times of the detailed analysis.

The high pressure point of the cycle, time 1, looks very similar for both mechanisms. Heat release is primarily concentrated in the shear layer. A noticeable difference between the marginally stable and unstable conditions is that there is no heat release in the cup region. This also highlights a difference between the two simulations, i.e., the burning of the fuel occurs further downstream for the detailed mechanism. There is unburnt fuel entering the combustor in both cases, combustion occurs in the shear layer further downstream for the detailed chemistry. Similar to the unstable case there is less unburnt methane in the recirculation region for the detailed chemistry.

As the pressure decreases so does the heat release, but not to the same extent that was observed in the unstable case. At times 2 and 3 both mechanisms show heat release primarily concentrated in the shear layer. At the low pressure point of the cycle, time 4, there is slightly less heat release in the detailed case, the fuel is also spending more time in the combustor before burning as evident by the heat release taking place further downstream compared to the global chemistry results. There is an increase in the amount of heat release as the pressure returns to high point. Both simulations predict this and there is very little discernable difference between the two simulations. The presence of excess fuel in the recirculation region with the global mechanism is also true for this case. This appears to be a minor effect since the same global behavior and

instability amplitudes are present. The similarity between the results from these two simulations suggests that the mixing is the controlling factor in this flow, and not the complexity of the kinetics.
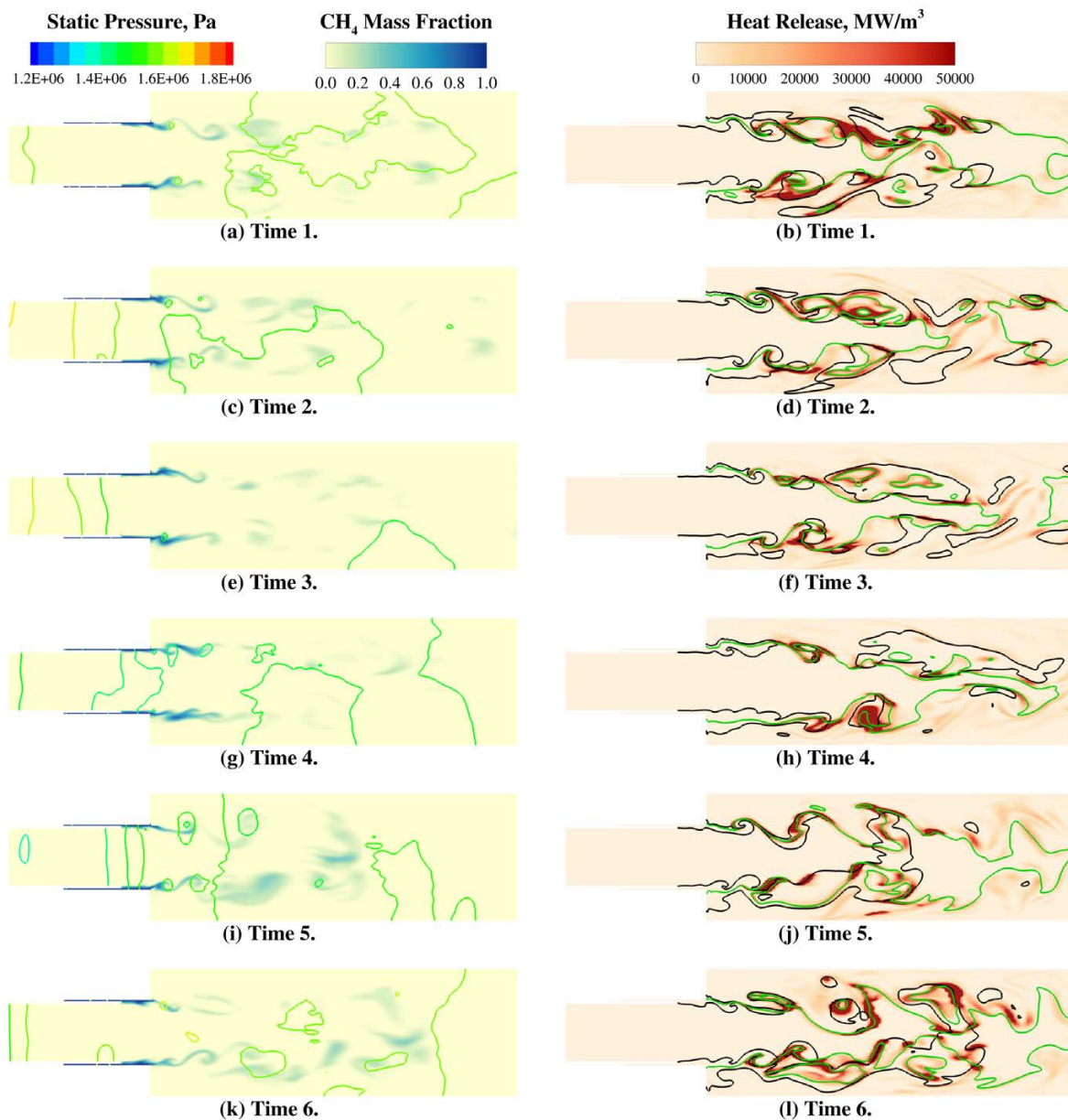


Figure 9: Detailed cycle analysis for the detailed chemistry for the marginally stable operating point. Images on the left show the fuel mass fraction contour, the lines represent pressure isobars. The images on the right show the heat release contour. The green line is a 2000 K isotherm and the black line is the stoichiometric mixture fraction.

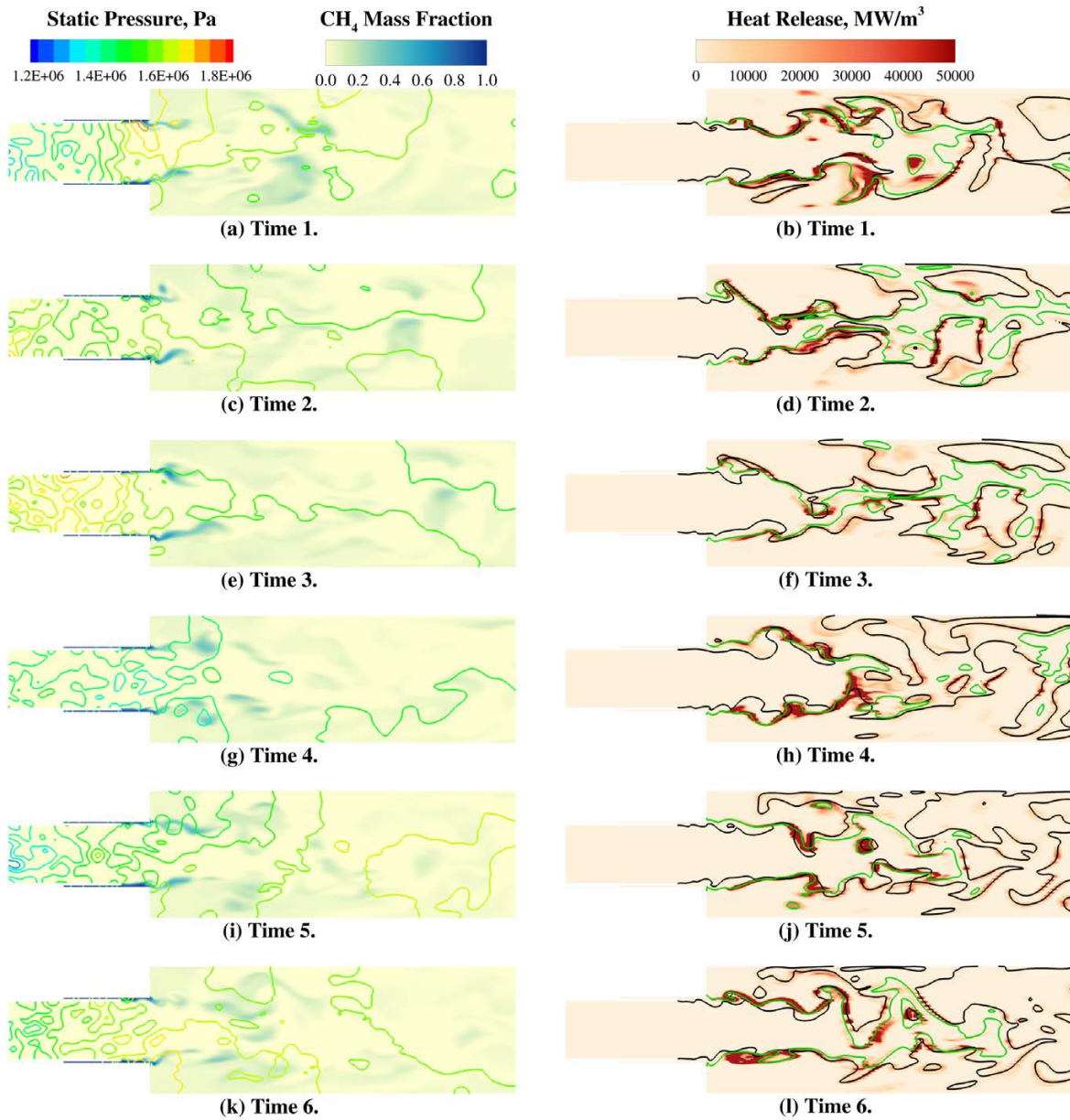American Institute of Aeronautics and Astronautics

Figure 10: Detailed cycle analysis for the global chemistry for the marginally stable operating point. Images on the left show the fuel mass fraction contour, the lines represent pressure isobars. The images on the right show the heat release contour. The green line is a 2000 K isotherm and the black line is the stoichiometric mixture fraction.

## IV.    Summary and Conclusions

A comparison between two chemical kinetics mechanisms—a single step global reaction and the 177 reaction GRI-Mech—was performed for the prediction of combustion instability in a single element shear coaxial injector. In all, four simulations were completed which covered two operating conditions: one marginally stable and one unstable. Under both operating conditions the amplitude of the unsteady pressure fluctuations was slightly higher for the detailed mechanism and there was also a decrease in the predicted frequency. The latter effect, in particular, brought the predicted frequencies to be closer to the experimentally observed values. The effect is due to an improved prediction of the temperature and composition of the combustion products, which in turn lowered the sound speed. The unstable condition was characterized by a cyclic heat release resulting from a temporary blockage of the incoming fuel. This effect was captured well by both kinetics mechanisms. Prior work based on two-dimensional simulations suggested that the detailed kinetics were important and showed a large increase in the amplitude for the simulations with the detailed kinetics compared to the global mechanism. It was speculated that the time to burn was incorrect and therefore did not properly couple with the chamber acoustics. The present work shows that this is not the case. The low amplitudes in the two-dimensional calculations are, in fact, attributable to poor mixing, and not the complexity of the chemical mechanism.

The behavior at both operation points is similar for both sets of kinetics. This indicates for this type of simulation the key aspect is the ability to capture effect of pressure on the heat release rate, which both mechanisms appear to be able to correctly capture. The fact that there were only small changes between the global and detailed chemistry also suggest that in this configuration that mixing is the dominant process controlling the combustion, and not the kinetics. There were some more subtle differences in the simulations. Both operating point showed considerably less fuel outside of the shear layer with the detailed mechanisms. There were also difference in the location of the heat release at the head end of the combustion but these appear to be secondary effects. Given that the detailed simulations required 22.5 times the amount of CPU core hours, we conclude that using detailed chemical kinetics is not warranted for the mixing-dominated operation that characterizes the shear-coaxial type of injector element and the associated flow conditions.

## Acknowledgments

## References

[1] Oefelein, J. and Yang, V., "Comprehensive Review of Liquid-Propellant Combustion Instabilities in F-1 Engines," *Journal of Propulsion and Power*, Vol. 9, No. 5, September-October 1993, pp. 657–677.

[2] Harvazinski, M., Huang, C., Sankaran, V., Feldman, T., Anderson, W., Merkle, C., and Talley, D., "Coupling between hydrodynamics, acoustics, and heat release in a self-excited unstable combustor," *Physics of Fluids*, Vol. 27, 2015, pp. 045102.

[3] Srinivasan, S., Ranjan, R., and Menon, S., "Flame Dynamics During Combustion Instability in a High-Pressure, Shear-Coaxial Injector Combustor," *Flow Turbulence and Combustion*, Vol. 94, No. 1, 2015, pp. 237–262.

[4] Garby, R., Selle, L., and Poinsot, T., "Large-Eddy Simulation of Combustion Instabilities in a Variable-length Combustor," *Comptes Rendus Mécanique*, Vol. 341, No. 1-2, 2013, pp. 220–229.

[5] Morgan, C., Shipley, K., and Anderson, W., "Comparative Evaluation Between Experiment and Simulation for a Transverse Instability," *Journal of Propulsion and Power*, Vol. 31, No. 6, 2015, pp. 1696–1706.

[6] Westbrook, C. and Dryer, F., "Simplified Reaction Mechanisms for the Oxidation of Hydrocarbon Fuels in Flames," *Combustion Science and Technology*, Vol. 27, 1981, pp. 31–43.

[7] Franzelli, B., Riber, E., Gicquel, L., and Poinsot, T., "Large Eddy Simulation of combustion instabilities in a lean partially premixed swirled flame," *Combustion and Flame*, Vol. 159, 2012, pp. 621–637.

[8] Sardeshmukh, S., Anderson, W., Harvazinski, M., and Sankaran, V., "Prediction of Combustion Instabilities with Detailed Chemical Kinetics," *53rd AIAA Aerospace Sciences Meeting*, Orlando, FL, Jan 2015, pp. 1–19, AIAA Paper 2015-1826.

[9] Sankaran, V. and Merkle, C., "Fundamental Physics and Model Assumptions in Turbulent Combustion Models for Aerospace Propulsion," *50th AIAA/ASME/SAE/ASEE Joint Propulsion Conference and Exhibit*, AIAA, Cleveland, OH, July 2014, pp. 1–14.

[10] Harvazinski, M., Talley, D., and Sankaran, V., "Comparison of Laminar and Linear Eddy Model Closures for Combustion Instability Simulations," *51st AIAA/SAE/ASEE Joint Propulsion Conference*, AIAA, Orlando, FL, July 2015, pp. 1–18.

[11] Frenklach, M., Wang, H., Goldenberg, M., Smith, G., Golden, D., Bowman, C., Hanson, R., Gardiner, W., and Lissianski,

V., "GRI-Mech—An Optimized Detailed Chemical Reaction Mechanism for Methane Combustion," Tech. Rep. GRI-95/0058, Gas Research Institute, 1995.

[12]Bowman, C., Hanson, R., Davidson, D., W.C. Gardiner, J., Lissianski, V., Smith, G., Golden, D., Frenklach, M., and Goldenberg, M., "GRI-Mech 2.11," .

[13]Smith, G., Golden, D., Frenklach, M., Moriarty, N., Eiteneer, B., Goldenberg, M., Bowman, C., Hanson, R., Song, S., W. Gardiner, J., Lissianski, V., and Qin, Z., "GRI-Mech 3.0," .

[14]Yu, Y., Sisco, J., Rosen, S., Madhav, A., and Anderson, W., "Spontaneous Longitudinal Combustion Instability in a Continuously-Variable Resonance Combustor," *Journal of Propulsion and Power*, Vol. 28, No. 5, 2012, pp. 876–887.

[15]Harvazinski, M., Anderson, W., and Merkle, C., "Analysis of Self-Excited Combustion Instability using Two- and Three-Dimensional Simulations," *Journal of Propulsion and Power*, Vol. 29, No. 2, 2013, pp. 396–409.

[16]Lian, C., Xia, G., and Merkle, C., "Solution-Limited Time Stepping to Enhance Reliability in CFD Applications," *Journal of Computational Physics*, Vol. 228, 2009, pp. 4836–4857.

[17]Li, D., Xia, G., Sankaran, V., and Merkle, C., "Computational Framework for Complex Fluids Applications," *3rd International Conference on Computational Fluid Dynamics*, Toronto, Canada, July 2004, pp. 619 – 624.

[18]Xia, G., Sankaran, V., Li, D., and Merkle, C., "Modeling of Turbulent Mixing Layer Dynamics in Ultra-High Pressure Flows," *36th AIAA Fluid Dynamics Conference and Exhibit*, San Francisco, CA, June 2006, pp. 1–17, AIAA Paper 2006-3729.

[19]Lian, C., Xia, G., and Merkle, C., "Impact of Source Terms on Reliability of CFD Algorithms," *Computers and Fluids*, Vol. 39, 2010, pp. 1909–1922.

[20]Wilcox, D., "Formulation of the $k$-$\omega$ turbulence model revisited," *AIAA Journal*, Vol. 46, No. 11, 2008, pp. 2823–2838.

[21]Harvazinski, M., Talley, D., and Sankaran, V., "Influence of Boundary Condition Treatment on Longitudinal Mode Combustion Instability Predictions," *49th AIAA/ASME/SAE/ASEE Joint Propulsion Conference and Exhibit*, AIAA, San Jose, CA, July 2013, pp. 1–14.

[22]Sisco, J., *Measurement and Analysis of Unstable Model Rocket Combustor*, Ph.d. Thesis, Purdue University, West Lafayette, IN, August 2007.